

Mitochondrial RNA granules are fluid condensates positioned by membrane dynamics

5 T. Rey^{1†*}, S. Zaganelli^{1,2†}, E. Cuillery¹, E. Vartholomaiou², M. Croisier³, J. Martinou^{2*}, S. Manley^{1*}

¹ Laboratory of Experimental Biophysics, École Polytechnique Fédérale de Lausanne (EPFL), Lausanne, Switzerland.

² Department of Cell Biology, University of Geneva, Genève, Switzerland.

10 ³ BioEM Core Facility and Technology Platform, Ecole Polytechnique Federale de Lausanne (EPFL), Lausanne, Switzerland

*Corresponding authors. Email: timo.rey@epfl.ch; jean-claude.martinou@unige.ch; suliana.manley@epfl.ch;

†these authors contributed equally

Supplementary Information

Supplementary Discussion

Further quantitative analysis of one and two-colour htSTORM-data

htSTORM acquisition and analysis were performed by adapting previously published workflows and analysis scripts as described by K. Douglass, and C. Sieben and colleagues^{17, 37}. **Extended**

25 **Data Fig. 1 a**, shows the composite workflow used for this study, where new, previously unpublished parts of the analysis are highlighted by asterisks.

Extended Data Fig. 1 b - f Show additional quantifications of MRG and nucleoid (mtDNA) architecture from STORM clustered localisations. MRGs were imaged using different markers (mtRNA, FASTKD2 and GRSF1), as indicated. mtDNA was used as a control. All plots show individual data points in grey, and box plots denote first and third quartiles as well as the median.

30 Whiskers comprise rest of distributions except outliers. Number (n) of clusters quantified for each

condition is represented in the figure. Multiple acquisitions, samples and imaging days were pooled. Two-sided Mann-Whitney-U test was used for statistical comparison to consider populations of unequal size. Number of granules analysed and median values are indicated in each figure. n.s. denotes p-values > 0.05 , * denotes p-values ≤ 0.05 , ** denote p-values ≤ 0.01 , *** denote p-values ≤ 0.001 , **** denote p-values ≤ 0.0001 . **Extended Data Fig. 1 b**, Eccentricity is used to describe how close a shape is to circular, where 1 describes a perfect circle, 2 describes an ellipse that is twice as long as wide, etc. Example shapes are represented in grey below the x-axis. Both MRG-proteins that we assessed form structures well-approximated as spheres, and their median eccentricity only differs slightly ($p = 5.1e^{-3}$), with largely overlapping boxes. Nucleoids and nascent RNA components of MRGs on the other hand, are significantly more elongated ($p_{\text{BrU-FASTKD2}} = 1.4e^{-15}$, $p_{\text{BrU-GRSF1}} = 1.7e^{-6}$). **Extended Data Fig. 1 c**, As an alternative way to compare the size of different components, foci area was determined as the area enclosed by the convex hull for each granule. Three outliers for FASTKD2 ($> 2.5 \mu\text{m}^2$) were removed for better visual comparison of the distribution, but included in numerical analysis. Consistent with **Extended Data Fig. 1 b, d**, MRG-protein foci are significantly larger than nascent-RNA foci ($p_{\text{BrU-FASTKD2}} = 2.7 \times 10^{-61}$, $p_{\text{BrU-GRSF1}} = 6.5 \times 10^{-49}$), yet less different from one another ($p_{\text{GRSF1-FASTKD2}} = 6.9 \times 10^{-7}$), as is visually apparent from the boxes' overlap. The distribution of mtRNA- and mtDNA-foci areas strongly overlap, though their medians are significantly different with $p_{\text{mtRNA-mtDNA}} = 1.2 \times 10^{-6}$. **Extended Data Fig. 1 d, and e**, Present alternative descriptors for the dimensions of point-clouds that are often used in single molecule localisation microscopy studies. The radius of gyration (R_g) is calculated as the root-mean-square of the distances between the cluster centre of mass and each localisation. The sigma was deduced as the average of the eigenvalues in two dimensions, and multiplied by two to yield a diameter. Like the FWHM in **Extended Data Fig. 1 b**, these measures

rely on statistics (variance of the distribution) and give less weight to individual signals. This makes them more robust towards outliers and thus preferred for size comparisons as opposed to the convex hull. By contrast, the convex hull may appear more intuitive when visualised and is less influenced by non-homogenous labelling of the structure of interest. It is important to understand that the true and exact size most likely lies somewhere in-between; which is why it is reassuring to find the same trend in size distributions by all techniques applied. **Extended Data Fig. 1 f**, To test whether protein foci are more dense than nucleic acid foci we determined their density of localisations as well as granularity (data not shown). The obtained data are difficult to interpret and do not allow conclusive statements. It is interesting to note however, that both GRSF1 and FASTKD2-foci follow a narrow normal distribution, while mtDNA & BrU show a much larger variance of density.

To allow comparison and correlation of two-colour htSTORM data **Extended Data Figure 2 a**, shows a montage with additional examples of two-colour htSTORM of MRGs (corresponding to **Extended Data Figure 1 c**). Scatter plots of localisations (right) are represented next to corresponding clusters of FASTKD2 (green) and mtRNA (BrU, blue) overlaid on widefield images (left). Convex hull areas are represented with dashed lines. The entire dataset analysed in **Extended Data Figure 1**, **Extended Data Figure 2** and **Supplementary Table 1** can be found on Zenodo. **Extended Data Figure 2 b**, and **Extended Data Figure 2 c**, Scatter plots for all FASTKD2-mtRNA (BrU) pairs, as well as a regression-fit with its standard deviation. Histograms of the distribution for FASTKD2 (y-axis, right, green), and mtRNA (x-axis, top, blue), including a kernel density estimate are shown. **Extended Data Figure 2 b**, Comparison of Diameter (FWHM) between FASTKD2 foci and BrU foci from individual granules (foci pairs) (n=26 MRGs over 4 independent experiments). We found no correlation ($R = 0.26$), indicating that granule size

defined by protein components does not linearly depend on nascent RNA size as visualised by BrU-incorporation. **Extended Data Figure 2 c**, Comparison of eccentricity (length/width) also showed no clear correlation between shape of BrU- and shape of FASTKD2-foci from individual granules (n=26 MRGs over 4 independent experiments). **Extended Data Figure 2 d-f**, Comparison of foci characteristics for one- versus two-colour htSTORM are shown to relate our two-colour htSTORM data to our one-colour measurements. We compared (Mann-Whitney-U test) the distribution of measurements of anti-BrU Alexa 647 stained and clustered granules from two-colour (n = 26 MRGs) to the one-colour data (n = 431 MRGs). We did the same for FASTKD2-foci, which were stained by anti-FASTKD2 DyLight 755 in two-colour and anti-FASTKD2 Alexa 647 in one-colour experiments. **Extended Data Figure 2 d**, comparison of FWHM showed no significant difference for FASTKD2 ($p = 0.22$) despite the differing secondary antibodies. For BrU foci, the two-colour data was significantly larger ($p = 8.8e^{-4}$) than the one-colour values reported in **Extended Data Figure 1**, using the same sample preparation and antibody strategy. A significant difference between two-colour-FASTKD2 and two-colour-mtRNA ($p = 0.0014$) on the other hand was still retained. **Extended Data Figure 2 e**, Comparison of eccentricity showed no significant difference between one-colour and two-colour populations of foci ($p_{\text{mtRNA}} = 0.36$, $p_{\text{FASTKD2}} = 1.0$) **Extended Data Figure 2 f**, When comparing size determined by convex hull, two-colour BrU-foci again differed from their one-colour counterparts ($p = 2.4e^{-4}$). We also found FASTKD2-size to differ significantly when assessed by convex hull ($p = 0.017$), though this may in parts be due to the heavy weight of two outliers as visible in the plot.

We interpret these results in the light of the slightly modified analysis pipeline. While both one-colour BrU- and FASTKD2-foci were selected solely for lying within focus, two-colour granules

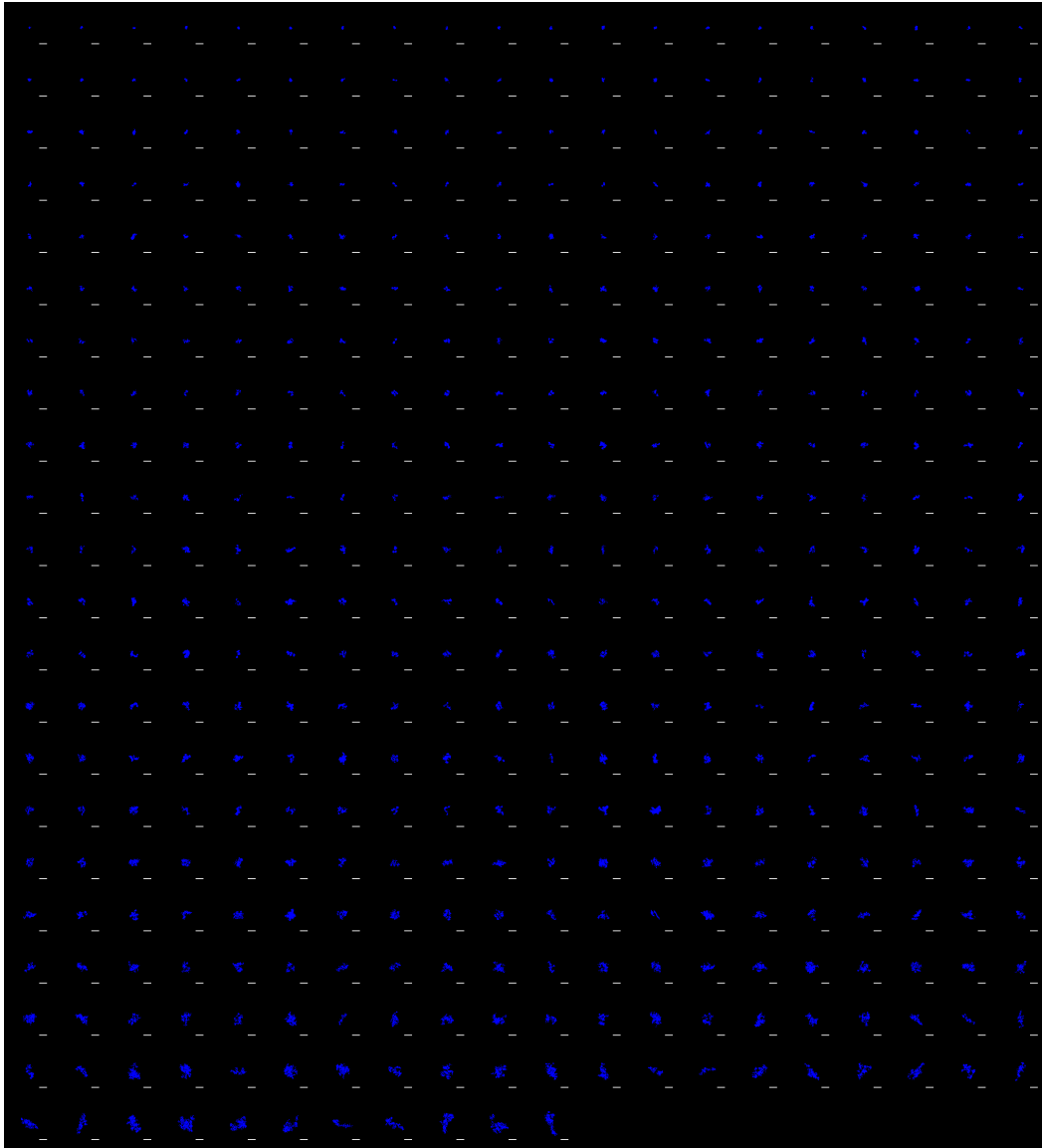
were selected to contain bright foci in both colours, thus likely over representing a particular subpopulation of MRGs. All plots show individual data points in grey, and box plots denote first and third quartiles as well as the median, whiskers comprise rest of distributions except outliers. Two-sided Mann-Whitney-U test was used for statistical comparison between populations of unequal size.

Membrane association and distribution of MRGs within mitochondria.

STED microscopy reveals ultrastructural alteration of cristae in cells treated with antimycin A. HeLa cells stably expressing Cox8a-SNAP as an inner membrane marker and FASTKD2-eGFP as an MRG marker were treated with 100 μ M antimycin A for 1 hour, STED live cell imaging as presented in **Extended Data Figure 6 a**. Kymographs below **Extended Data Figure 6 b-c** highlight the co-mobility of individual granules In **Extended Data Figure 6 e**, and **f**, Histograms of the absolute or relative position of MRGs within their host mitochondria and simulated, randomly positioned granules show the observed distribution of MRG positions is not significantly different from a simulated random distribution. MRGs are thus randomly placed within mitochondria.

Supplementary Figures

mtRNA (BrU) clusters after DBSCAN clustering analysis (n=431)

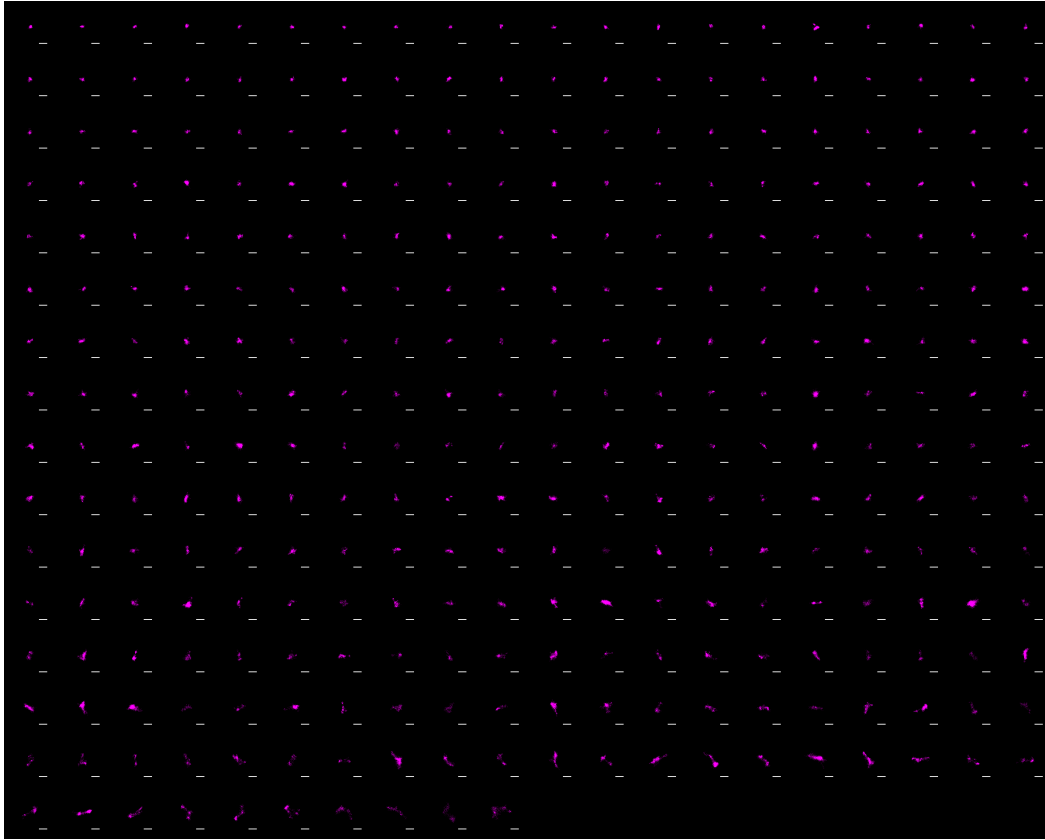


Supplementary Fig. 1: Montage of mtRNA granules imaged with htSTORM (one color).

5

Montage of 431 granules after DBSCAN clustering of MRGs immunolabeled using anti-BrdU antibody, following a 1h bromouridine incubation of live cells prior to fixation. These data correspond to those presented in **Fig. 1b**. Scale bars: 200 nm.

mtDNA clusters after DBSCAN clustering analysis (n=310)

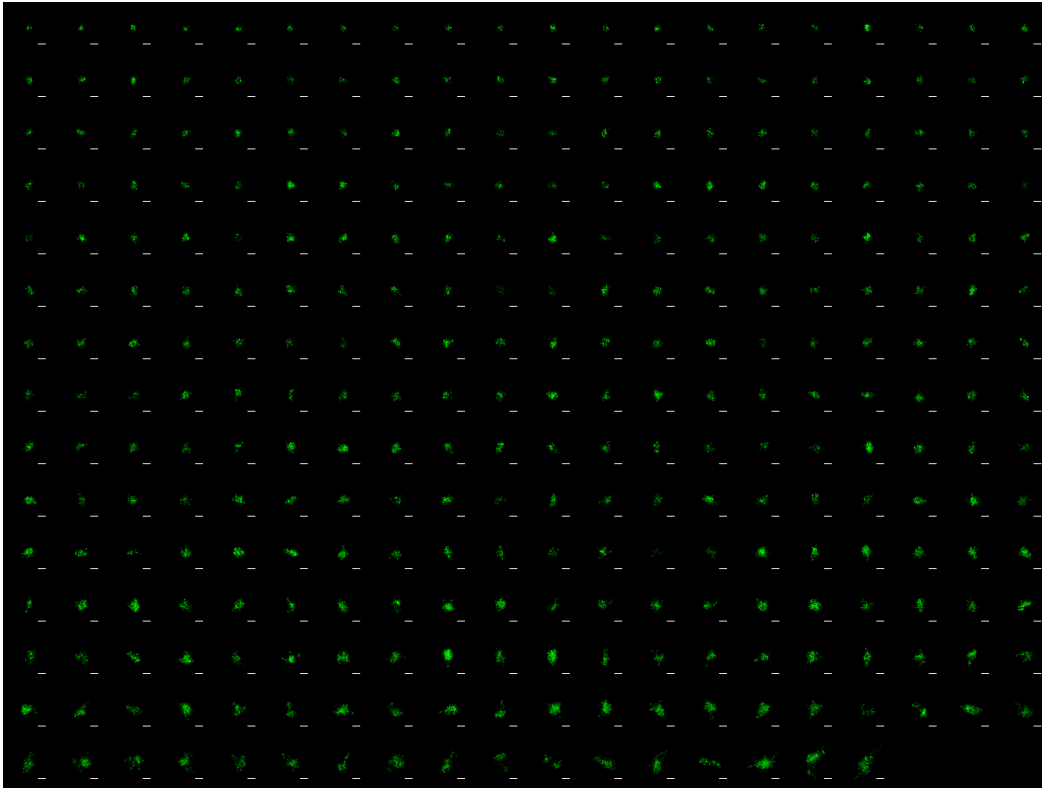


Supplementary Fig. 2: Montage of mtDNA granules imaged with htSTORM (one color).

Montage of 310 granules after DBSCAN clustering of nucleoids immunolabeled using anti-DNA antibody. These data correspond to those presented in **Fig. 1b**. Scale bars: 200 nm.

5

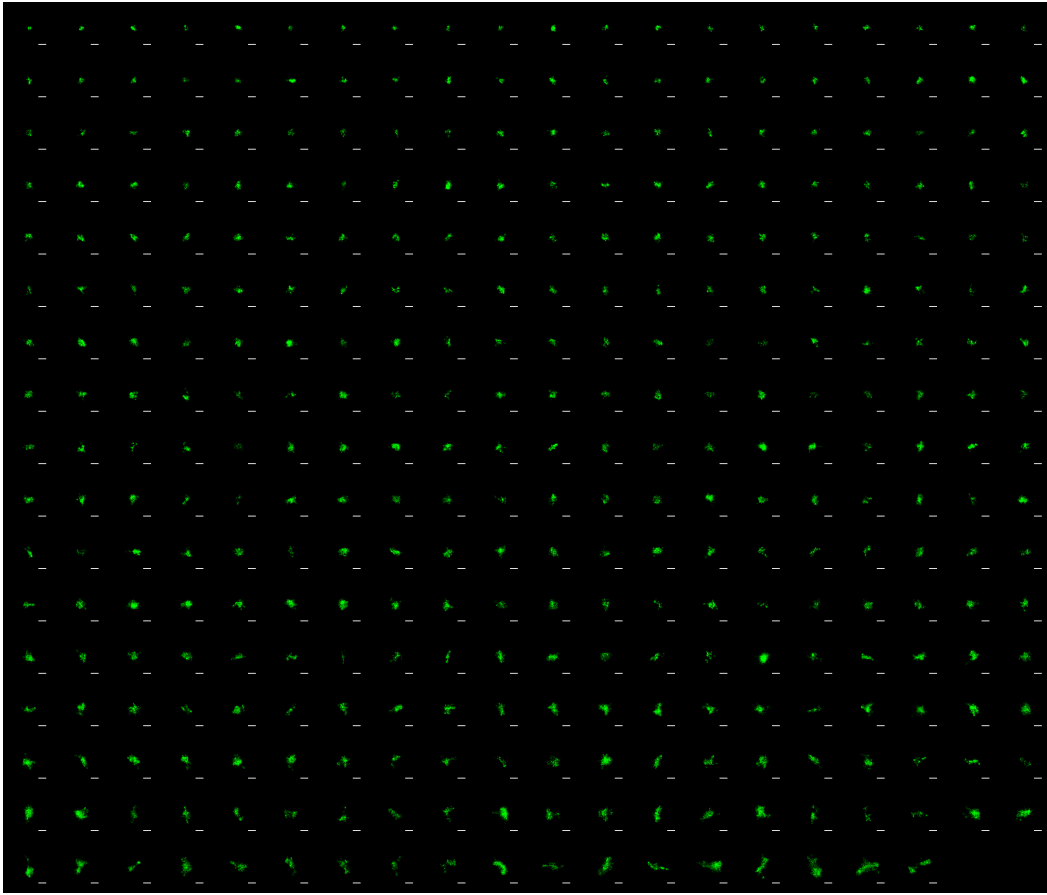
FASTKD2 clusters after DBSCAN clustering analysis (n=297)



Supplementary Fig. 3: Montage of FASTKD2 granules imaged with htSTORM (one color).

Montage of 297 granules after DBSCAN clustering of MRGs immunolabeled using anti-FASTKD2 antibody. These data correspond to those presented in **Fig. 1b**. Scale bars: 200 nm.

GRSF1 clusters after DBSCAN clustering analysis (n=338)



Supplementary Fig.4: Montage of GRSF1 granules imaged with htSTORM (one color).

Montage of 338 granules after DBSCAN clustering of MRGs immunolabeled using anti-GRSF1 antibody. These data correspond to those presented in **Fig. 1b**. Scale bars: 200 nm.